

Hubble Space Telescope imaging of the progenitor sites of six nearby core-collapse supernovae

J.R. Maund^{1*} and S.J. Smartt²

¹*Institute of Astronomy, University of Cambridge, Madingley Road, Cambridge CB3 0HA, England, U.K.*

²*Department of Physics and Astronomy, Queen's University Belfast, Belfast, BT7 1NN, Northern Ireland, U.K.*

11 November 2018

ABSTRACT

The search for the progenitors of six core-collapse supernovae (CCSNe) in archival HST WFPC2 pre-explosion imaging is presented here. These SNe are 1999an, 1999br, 1999ev, 2000ds, 2000ew and 2001B. Post-explosion imaging of the SNe, with the HST ACS/WFC, has been utilised with the technique of differential astrometry to identify the progenitor locations on the pre-explosion imaging. SNe 1999br, 1999ev, 2000ew and 2001B are recovered in late time imaging and an estimate of the progenitor location on the pre-explosion imaging, with sub-pixel accuracy, has been made. Only the progenitor of the type II-P SN 1999ev has been recovered, on pre-explosion F555W imaging, at a 4.8σ significance level. Assuming a red supergiant progenitor, the pre-explosion observation is consistent with $M_{ZAMS} = 15 - 18M_{\odot}$. The progenitors of the other five SNe were below the 3σ detection threshold of the pre-explosion observations. The detection thresholds were translated to mass limits for the progenitors by comparison with stellar evolution models. Pre-explosion observations of the peculiarly faint SN 1999br limit the mass of a red supergiant progenitor to $M_{ZAMS} < 12M_{\odot}$. Analysis has been extended, from previous studies, to include possible detections of high- T_{eff} , high-mass stars by conducting synthetic photometry of model Wolf-Rayet star spectra. The mass limits for the type II-P SNe 1999an and 1999br are consistent with the previously determined mass limits for this type of SN. The detection limits for the progenitors of the type Ibc SNe (2000ds, 2000ew and 2001B) do not permit differentiation between high-mass WR progenitors or low mass progenitors in binaries.

Key words: stars : evolution – supernovae : general – supernovae : individual : 1999an – supernovae : individual : 1999br – supernovae : individual : 1999ev – supernovae : individual : 2000ds – supernovae : individual : 2000ew – supernovae : individual : 2001B – galaxies : individual : IC 755 – galaxies : individual : NGC 4900 – galaxies : individual : NGC 4274 – galaxies : individual : NGC 2768 – galaxies : individual : NGC 3810 – galaxies : individual : IC 391.

1 INTRODUCTION

Supernovae (SNe) are associated with the end points of the evolution of particular types of stars. Stars with initial masses $> 8M_{\odot}$ are believed to undergo a core-collapse induced explosion at the end of their lives (Heger et al. 2003). SNe are important drivers of the chemical and physical evolution of their host galaxies: distributing heavy elements newly synthesised in the explosion and injecting kinetic and radiative energy into the surrounding medium (Thielemann et al. 2003). The type of the SN depends on the evolutionary status of the progenitor object just prior to core-collapse. The observational identification of these ob-

jects, and determination of their nature, is of importance to the study of the evolution of massive stars and the evolution of SNe (Hamuy & Pinto 2002).

SNe are principally classified by the absence (Type I) or presence (Type II) of H α features in their early time optical spectral. SNe are further sub-classified by other spectral features or the shapes of their light curves. The type Ia SN class is very homogeneous, characterized by the presence of a Si II absorption feature (Filippenko 1997). SN Ia occur in old-intermediate age stellar populations (in E, S0 and the bulges of S galaxies) composed of low-intermediate mass stars. SN Ia are thought to arise from the thermonuclear explosion of either C-O white dwarfs accreting material from a binary companion or the coalescence of two C-O white dwarfs in a close binary (Branch et al. 1995). The Si II absorption fea-

* Email: jrm@ast.cam.ac.uk

ture is not seen in types Ib/c. SN Ib show spectral features due to He, while SN Ic are He deficient. These SNe, along with all type II SNe, are seen in young blue star forming regions in the spiral arms of late type galaxies and are associated with massive star progenitors ($M_{ZAMS} > 8M_{\odot}$) undergoing a core-collapse induced explosion. The absence of H, and the subsequent absence of He in SN Ic, is associated with increasing mass loss, and hence initial mass, of the progenitor or enhanced mass loss due to a binary interaction (Podsiadlowski et al. 2004). Type IIP/L SNe show prominent features due to H. SN IIP exhibit a plateau feature in their light curves, due to the expansion and recombination of a large H-rich envelope, as well as H Balmer P-Cygni profiles in their optical spectra (Hamuy 2003). The progenitors for these objects are likely to be stars towards the lower range of the masses that will produce a core-collapse SN, for which mass loss is not significant allowing the H-envelope to be retained. Smartt et al. (2003) presented initial mass limits, from pre-explosion imaging, for a number of type IIP SN progenitors, suggesting the progenitors were all stars with initial mass $< 15M_{\odot}$. The detected progenitor of the IIP SN2003gd an M0 supergiant, had an initial mass $8_{-2}^{+4}M_{\odot}$, consistent with the theoretical minimum initial mass for a core-collapse SN (Smartt et al. 2004). SN IIL are thought to arise for slightly more massive stars ($\sim 20M_{\odot}$) for which mass loss is much more important. In these cases the stars have retained an H-envelope of mass $\sim 1 - 2M_{\odot}$, which is not massive enough to produce a plateau and so the SN light curve decays linearly (Turatto 2003). In addition there are a number of type II subclassifications which are classified by spectroscopic features. Type IIB SNe transform from a type II to a Ib SN, of which SN1993J was the class prototype. The transition is due the retention of thin veil of the H envelope which gives rise to the initial classification of type II, but upon dissipation transforms to Ib. Low velocity IIn SNe exhibit narrow spectral lines. This may be due to collision of the SN with a dense circumstellar medium (e.g. 1998S, Lentz et al. 2001) or the eruptions of Luminous Blue Variables (e.g. 1997bs, Van Dyk et al. 2000) which appear similar to CCSNe.

Core-collapse SNe (CCSNe) are a heterogenous group due to the different permutations of the explosion. In the cases of single star progenitors the sequence IIP→IIL→IIB→Ib/c (Heger et al. 2003) can be considered to be due to increasing initial mass, and hence mass loss during the final stages of evolution. The outer H rich and subsequently He rich layers are stripped due to the increasing levels of mass loss. The role of binaries, and in particular mass and angular momentum exchange, provide alternative routes for different mass progenitors to appear as the same SN type (Maund et al. 2004). The direct determination of the nature of an SN progenitor requires observations of the progenitor prior to explosion. In most cases this is from fortuitous imaging available from telescope archives which was acquired for some other purpose, but has also imaged the SN location. Given the rarity and randomness of CCSNe it is necessary to look to nearby galaxies ($< 20\text{Mpc}$) in order to observe enough events at a feasible rate, coupled with a reasonable probability of detecting the progenitor and resolving it from neighbouring stars. A multi-wavelength deep imaging survey of nearby galaxies has been undertaken by the authors to improve the likelihood of appropriately deep and high reso-

lution pre-explosion data being available for future nearby SNe.

In only three cases have the progenitors of definite CCSNe, with their parameters fully determined, been identified in pre-explosion frames: 1987A (Gilmozzi et al. 1987), 1993J (Aldering et al. 1994) and 2003gd (Smartt et al. 2004). SN1987A in the Large Magellanic Cloud (LMC) was noted as a peculiar type II SN and the progenitor star was identified as Sk $-69^{\circ}202$ (Walborn et al. 1989) a B3Ia star. SN1993J was the prototypical type IIB SN, in M81, and the progenitor was identified as K0Ia star with an unknown ultraviolet component (Aldering et al. 1994). Neither of these progenitors is consistent with the canonical M-supergiant progenitor predicted for these types of SNe. In both cases, however, there is evidence that binarity plays a particularly important role. Podsiadlowski & Joss (1989) describe a binary model for the progenitor of SN 1987A and Maund et al. (2004) report the discovery of a blue supergiant companion to the progenitor of SN 1993J. The detected progenitor of SN 2003gd was the first red supergiant progenitor observed for a type IIP SN. In a number of cases pre-explosion imaging of the SN location has been available in a number of archives, in particular that of the Hubble Space Telescope (HST), but the pre-explosion images were not deep enough to detect the progenitor. In these cases Smartt et al. (2002, 2001, 2003) have placed brightness limits on the progenitors given the limiting magnitude of the pre-explosion frames at the SN position. The brightness limits have then been translated to mass limits by plotting the detection threshold on the Hertzsprung-Russell diagram and determining the mass range for which the progenitor would not have been detected in the pre-explosion image. Smartt et al. (2002, 2001, 2003) have used post-explosion imaging of the SN, with the technique of differential astrometry, to locate the SN position on pre-explosion images to sub-pixel accuracy. Van Dyk et al. (2003) have similarly attempted to identify progenitors in pre-explosion imaging. They have used the reported positions of SNe, such as given in IAU Circulars. The correct identification of progenitors is limited, however, by the poor pointing accuracy of HST (requiring the astrometric re-calibration of pre-explosion frames) and uncertainties in the reported positions of SNe.

The parameters of the progenitor may also be estimated, using various calibrations, from the evolution of the SN itself. The light curves and velocity evolution of the SNe have been used, with particular theoretical calibrations, to determine the ejected and Ni masses (Hamuy 2003). Epochs of mass loss have been probed by observing the variations in the radio light curves of certain SN due to the interaction of the SN with the progenitor's circumstellar medium (Ryder et al. 2004). Direct detection of the progenitor, whilst being a reliable method of determining the progenitor parameters, is also a useful check and calibration for the other techniques for determining the properties of the progenitors from the SN.

In this paper we present the search for the progenitors of six nearby CCSNe: 3 type IIP SNe (1999an, 1999br and 1999ev), 2 type Ib SNe (2000ds and 2001B) and 1 type Ic (2000ew). Fortuitous pre-explosion WFPC2 imaging for these SNe is available in the Hubble Space Telescope (HST) archive. The host galaxies of these SNe lie within 26Mpc, increasing the likelihood of detecting and resolving individual stars. The

Table 1. A table listing the properties of the SNe and their host galaxies discussed in this study.

SN	SN type	Host galaxy	Type	μ	i
1999an	II	IC 755	SBb	31.79	90
1999br	IIpec	NGC 4900	SBc	30.82	16.5
1999ev	II	NGC 4274	SBab(r)	30.96	71.8
2000ds	Ib	NGC 2768	E-Sa	31.84	90
2000ew	Ic	NGC 3810	Sc	30.90	47.8
2001B	Ib	IC 391	Sc	32.07	11.14

μ Kinematical distance modulus quoted by LEDA, assuming $H_0 = 70 \text{ km s}^{-1}$.

i Inclination angle of the plane of the galaxy quoted by LEDA.

properties of these SNe, and their host galaxies¹, are presented in table 1. The analysis of pre- and post-explosion imaging of these SNe (photometry, differential astrometry and determination of the limiting magnitudes) is presented in §2. §3 presents the results of the observations for each of the six SNe in this study. These results will be discussed, in the context of the parameters of the progenitors, in §4. We adopt the technique of Smartt et al. (2001, 2002, 2003) to place mass limits on the progenitors. Van Dyk et al. (2003) have attempted progenitor detection of these SNe in the publicly available WFPC2 images. They claim possible detections of the progenitors of SNe 1999br, 1999ev and 2001B. We show, however, that the only progenitor recovered is that of the type II SN 1999ev.

2 OBSERVATIONS AND DATA ANALYSIS

2.1 Pre- and post-explosion WFPC2 images

Hubble Space Telescope (HST) Wide Field Planetary Camera 2 (WFPC2) observations of the SN location acquired prior to explosion were identified using the ST-ECF ASTROVIRTEL *Querator* tool². This tool identifies exposures for which the target falls on the field of view, taking into account the peculiar mosaic shape of the WFPC2. The data was passed through the On-the-fly-recalibration (OTFR) pipeline and retrieved from the ST-ECF archive. A journal of these observations is presented as table 2. In addition a number of post-explosion WFPC2 images of the SNe were available and these are listed in table 3. The post-explosion frames were reduced and analysed in a similar manner to the pre-explosion images. Individual cosmic ray exposures were combined under IRAF using the STSDAS *crrej* routine. Image shifts, in the cases of dithered observations, were adopted from the WFPC2-B association tables and applied to bring the images to a common origin. Shifts were made with the IRAF task *imshift*. The combined and distortion corrected images were photometered using the IRAF implementation of the DAOPHOT package (Stetson 1987). Point spread function (PSF) models, taking into account variations across and between individual chips, were created using the TINYTIM program (Krist & Hook 2004) and were used in the photometry task ALLSTAR. Aperture and charge transfer efficiency

corrections (Holtzman et al. 1995; Dolphin 2000a) were applied to the output photometry. The output STMAG magnitudes were converted to the VegaMag system using the latest zeropoints of Dolphin (2000a)³. The positions of stars, output by DAOPHOT, were utilised to recalibrate the absolute astrometry of the WFPC2 frames and align groups of images of the same galaxy. The recalibration of the absolute astrometry and the technique of differential astrometry is discussed in §2.3.

2.2 Post-explosion ACS images

Post-explosion observations of these SNe were conducted as part of our program GO9353 (PI: S. Smartt) for HST cycle 11, with the HST Advanced Camera for Surveys (ACS) Wide Field Camera (WFC). Observations were conducted in three broad-band filters: F435W, F555W and F814W. A journal of these observations is presented in table 3. Images, passed through the OTFR pipeline, were retrieved from the ST-ECF archive. A grid of PSF models for both WFC chips and for each set of filters used were constructed using the TINYTIM program. Photometry was then conducted using the DAOPHOT ALLSTAR routine. Empirical aperture corrections were calculated, for each frame individually, to a radius of $0.5''$. A correction was made for the charge transfer efficiency following the prescription of Riess & Mack (2004), adopting the updated distortion coefficients⁴ of Cox & Mack (2004). The stellar photometry was then converted to standard Johnson-Cousins B, V and I magnitudes utilising the relationships of Holtzman et al. (1995), since the ACS photometric system is calibrated to within 0.03 magnitudes of the corresponding filters in the WFPC2 photometric system (Pavlovsky 2004).

2.3 Astrometry

The pointing accuracy of HST, and hence the absolute astrometric accuracy of HST imaging, is of the order $1\text{--}2''$ (Smartt et al. 2003). In addition the accuracy of the reported SN positions is $\sim 0.5\text{--}1''$. This amounts to a potential error of $3''$ or 30 WF pixels on WFPC2. Van Dyk et al. (2003) have utilised catalogued positions of stars which fall on the pre-explosion images to recalibrate the absolute astrometry and compensate for the uncertainty in HST pointing. The uncertainty of the reported SN position is, however, still present. In crowded fields, therefore, better astrometry is necessary to provide a more secure identification of the progenitor object. Smartt et al. (2001, 2002, 2003) have utilised purposefully acquired post-explosion imaging to provide an accurate position for the progenitor object on pre-explosion images using the technique of differential astrometry. The transformation between the pre- and post-explosion frames, using stars common to both images, allows the determination of the SN location on the pre-explosion image. In this study the technique of differential astrometry is preferentially used if the SN has been recovered in the post-explosion frames. The astrometry of the pre-explosion WFPC2 images were re-calibrated, in cases when the SN

¹ <http://www-obs.univ-lyon1.fr/hypercat/>

² <http://archive.eso.org/querator/>

³ http://www.noao.edu/staff/dolphin/wfpc2_calib

⁴ <http://www.stsci.edu/hst/acs/analysis/PAMS>

Table 2. Summary of pre-explosion data

SN	Date of Observation	Dataset	Filter	Total Exposure Time (s)	HST program
1999an	1995 Jan 05	U29R3R01/02	F606W	160	GO-5446
1999br	1995 Jan 29	U29R2N01/02	F606W	160	GO-5446
1999ev	1995 Feb 05	U2JF0101/02/03	F555W	296	GO-5741
2000ds	1995 Dec 04	U2TV1803	F555W	160	GO-5999
	1995 Dec 04	U2TV1801/02	F814W	320	GO-5999
	1998 May 20	U3M71605/06	F555W	1000	GO-6587
	1998 May 20	U3M71608/09	F814W	2000	GO-6587
2000ew	1994 Nov 04	U29R1R01/02	F606W	160	GO-5446
2001B	1994 Feb 21	U2920B01	F555W	70	GO-5104

Table 3. Summary of post-explosion data

SN	Date of Observation	Dataset	Filter	Total Exposure Time (s)	Instrument	HST program
1999an	2002 Jul 12	J8DT05030	F435W	400	ACS/WFC	GO-9353
	2002 Jul 12	J8DT05010	F555W	430	ACS/WFC	GO-9353
	2002 Jul 12	J8DT05030	F814W	430	ACS/WFC	GO-9353
1999br	2002 Jun 20	U6EA8601/02	F450W	460	WFPC2	GO-9042
	2002 Jun 20	U6EA8603/04	F814W	460	WFPC2	GO-9042
	2002 Dec 23	J8DT06030	F435W	400	ACS/WFC	GO-9353
	2002 Dec 23	J8DT06010	F555W	430	ACS/WFC	GO-9353
	2002 Dec 23	J8DT06020	F814W	430	ACS/WFC	GO-9353
1999ev	2002 Dec 31	J8DT03030	F435W	400	ACS/WFC	GO-9353
	2002 Dec 31	J8DT03010	F555W	450	ACS/WFC	GO-9353
	2002 Dec 31	J8DT03020	F814W	450	ACS/WFC	GO-9353
2000ds	2002 May 31	J8DT02030	F435W	680	ACS/WFC	GO-9353
	2002 May 31	J8DT02010	F555W	700	ACS/WFC	GO-9353
	2002 May 31	J8DT02020	F814W	700	ACS/WFC	GO-9353
2000ew	2001 Nov 07	U6EA5401/02	F450W	460	WFPC2	GO-9042
	2001 Nov 07	U6EA5403/04	F814W	460	WFPC2	GO-9042
	2002 Jun 26	J8DT04030	F435W	400	ACS/WFC	GO-9353
	2002 Jun 26	J8DT04010	F555W	430	ACS/WFC	GO-9353
	2002 Jun 26	J8DT04020	F814W	430	ACS/WFC	GO-9353
2001B	2002 Jun 09	J8DT01020	F435W	800	ACS/WFC	GO-9353
	2002 Jun 09	J8DT01010	F555W	700	ACS/WFC	GO-9353
	2002 Jun 09	J8DT01030	F814W	700	ACS/WFC	GO-9353

was not recovered, using stars catalogued in the USNO-B1.0 (Monet et al. 2003) and Automated Plate Machine (APM, Irwin & McMahon 1992) catalogues. The astrometric precisions of these catalogues are quoted as $0.2''$ and $0.1''$ respectively. The pre- and post-explosion images were aligned, by identifying common stars in both frames, using the positions calculated by DAOPHOT. The transformations between images were calculated using the *geomap* task in IRAF. The absolute astrometry of the images were recalibrated using the *ccmap* and *ccsetwcs* tasks. All positions

quoted in this study are J2000.0. The plate scales of the WF and PC chips of WFPC2 are $0.1''$ and $0.05''$ respectively. The ACS WFC has the same plate scale as the WFPC2 PC chip. Photometry and astrometry were conducted on the original data frames, but for the purposes of comparison all the images presented here have been translated, rotated and scaled to be consistent with the coordinates of the ACS WFC post-explosion images.

2.4 Detection limits of pre-explosion WFPC2 images

In the cases when the progenitor was not detected in the pre-explosion frames the detection limit of the images was determined in order to place a brightness limit on the progenitor. The brightness of the background was measured using aperture photometry. The properties of the background were then used to estimate the stellar flux required for a detection of 3σ . The signal-to-noise ratio for a photometered star is given by:

$$S/N = \frac{F_{star}}{\sqrt{F_{star} + Q}} \quad (1)$$

where F_{star} is the flux of the star in electrons and Q represents the noise contribution from the background and readnoise. Q is given by:

$$Q = A_{star} \left(1 + \frac{A_{star}}{A_{sky}} \right) (F_{sky} + R^2) \quad (2)$$

F_{sky} is the average flux of a sky pixel. A_{star} and A_{sky} are the respective areas of the aperture and sky annulus in pixels. R is the read noise in electrons, which for the WFPC2 images summed with *crrej* is given by the sum, in quadrature, of the read noises of the individual frames. The calculation for the signal-to-noise ratio may be inverted, given the sky background as measured by the aperture photometry, to determine the flux of star at the detection threshold.

$$F_{star} = \frac{1}{2} S/N \sqrt{S/N^2 + 4Q} + \frac{1}{2} S/N^2 \quad (3)$$

In this study the threshold will be taken as $S/N = 3$. The limiting magnitude was then calculated in the standard manner taking into account the corrections for the VegaMag zeropoint, aperture size and charge transfer efficiency.

2.5 Estimates of reddening

The post-explosion photometry of stars, in the direct vicinity of the SN, was utilised to determine a reddening along the line of sight. This simultaneously takes into account the contribution of the internal reddening and the foreground reddening. Independent values of the foreground reddening were adopted from the NASA/IPAC Extragalactic Database (NED)⁵, after Schlegel et al. (1998). The apparent colours, $B - V$ and $V - I$, of stars within $6''$ of each SN were compared against a standard supergiant intrinsic colour sequence, from Drilling & Landolt (2000). The displacement of the stars' apparent colours from the intrinsic supergiant colour sequence was calculated along the reddening vector, adopting a standard Cardelli et al. (1989) and O'Donnell (1994) reddening law. Intermediate values in the supergiant intrinsic colour sequence were estimated using linear interpolation. The displacement D between the apparent and intrinsic colours of the stars was related to the reddening by:

$$\begin{aligned} D^2 &= ((B - V) - (B - V)_0)^2 + ((V - I) - (V - I)_0)^2 \\ &= (E(B - V))^2 + (E(V - I))^2 \\ &= (1 + \alpha)^2 (E(B - V))^2 \end{aligned} \quad (4)$$

For a Cardelli et al. (1989) reddening law, with $R_V = 3.1$, $\alpha = 0.62$. A weighted mean value of the reddenings of all the stars was adopted as the total reddening towards the SN. The extinctions in the WFPC2 band-passes were calculated, from A_V , using the ratios of extinctions of Schlegel et al. (1998). The precision of this technique is limited by the quality of the photometry and hence the number of bright nearby stars considered. This technique indicates, however, when the reddening appropriate for the SN is much higher than the foreground reddening alone. This is particularly important when considering the complicated line of sight to SNe in galaxies with large inclinations.

3 OBSERVATIONAL RESULTS

3.1 SN 1999an

SN 1999an was discovered on 1999 March 7.83 UT (Wei et al. 1999) in the SBb galaxy IC 755 and the presence of strong H Balmer P Cygni profiles showed it to be a classical type II SN. Sarneczky et al. (1999) noted the position of the SN as $\alpha = 12^{\text{h}}01^{\text{m}}10^{\text{s}}.57$, $\delta = +14^{\circ}06'12''.3$. Van Dyk et al. (2003) independently quote a position $\alpha = 12^{\text{h}}01^{\text{m}}10^{\text{s}}.57$, $\delta = +14^{\circ}06'11''.1$ with a conservative uncertainty of $\pm 0.4''$. A 160s pre-explosion F606W WFPC2 image, acquired 3.2 years prior to discovery (program GO-5446, PI: G. Illingworth), was available in the HST archive. The SN location was re-imaged with the ACS/WFC, in three colours, 3.3 years after discovery. The coordinate transformation between the pre-explosion frame and the post-explosion F555W image was calculated, with an uncertainty of 0.46 WF pixels (WFPC2) or $0.046''$. The pre-explosion frame, due to a more advantageous orientation including six USNO-B1.0 stars, was astrometrically recalibrated. The absolute astrometric accuracy was $0.42''$. The SN location occurred on the WF2 chip of the pre-explosion image. The total uncertainty of the SN position was $0.62''$ or 6 WF pixels. The SN location on the pre- and post-explosion images is shown as figure 1. There is no noticeable difference between the pre- and post-explosion images within the error circle of the SN location. This suggests that the progenitor is not detected in the pre-explosion image and the SN is not recovered on the post-explosion image to limiting magnitudes of $m_{F435W} = 26.2 \pm 0.5$, $m_{F555W} = 26.0 \pm 0.4$ and $m_{F814W} = 25.5 \pm 0.4$. The limiting magnitude at the SN location on the pre-explosion image was determined to be $m_{F606W} = 24.7 \pm 0.2$. IC 755 is almost exactly edge on with evidence for bar feature (Lütticke et al. 2000). This implies that the internal reddening towards SN1999an and its progenitor is likely to be higher than the NED quoted foreground reddening $E(B - V) = 0.032$. The reddening, including the internal contribution, determined from nearby stars was $E(B - V) = 0.13 \pm 0.06$. This implies an absolute extinction of $A_{F606W} \approx A_V = 0.42$. At the distance of IC 755, 22.8Mpc, this gives a limiting absolute magnitude of $M_{F606W} \geq -7.48$.

3.2 SN 1999br

SN 1999br was discovered on 1999 April 12.4 in the galaxy of NGC 4900 by King (1999). The presence of

⁵ <http://nedwww.ipac.caltech.edu/>

Figure 1. Pre- and post-explosion images of the site of SN 1999an in IC 755. (a) WFPC2 F606W 160s exposure, acquired on 1995 January 5, scaled and rotated to coordinates of ACS/WFC observations, (b) ACS/WFC F555W 430s exposure acquired on 2002 July 12 and (c) an ACS/WFC F814W 430s exposure acquired at the same epoch as the F555W image. The uncertainty in the SN position, from the quoted absolute astrometry, is indicated by the black circle. - see jpeg

Figure 3. Pre- and post-explosion imaging of the site of SN 1999br in the NGC 4900. (a) Post-explosion ACS/WFC F555W image showing an object detected at the location of SN1999br. (b) Pre-explosion WFPC2 F606W image. The SN location is indicated, with the positional uncertainty of $0.3''$ (6 ACS/WFC pixels or 3 WFPC2 WF3 pixels), by the circle. The cross hairs indicate the object suggested by Van Dyk et al. (2003) as the likely progenitor. (c) TNG/OIG V-band image of SN 1999br. The position of the SN on this image was used to provide an independent location of the SN on pre-explosion and later post-explosion imaging. (d) Post-explosion WFPC2 PC F814W image of the SN location. The SN is not detected, 3.14 years after discovery, with a limiting magnitude of $m_{F814W}(3\sigma) = 24.33$. - see jpeg

broad Balmer lines showed this to be an early Type II SN (Garnavich et al. 1999), although the the relative strengths of these lines indicated that it was sub-luminous (Filippenko et al. 1999). Patat et al. (1999) found that the expansion velocities of this SN were much lower than normal Type II SNe and similar to the low-energy SN 1997D. Photometric observations by Pastorello et al. (2004) showed a plateau in the light curve, classifying 1999br as a type II-P SN. King (1999) gives the location of the SN as $\alpha = 13^{\text{h}}00^{\text{m}}41^{\text{s}}.80$, $\delta = +2^{\circ}29'45''.8$. The SN position was imaged with HST WFPC2, with a 160s F606W exposure, 4.16 years prior to explosion (program GO-5446, PI: G. Illingworth). WFPC2 and ACS images of the SN were acquired 3.19 and 3.70 years after explosion respectively. The absolute astrometry of the three colour ACS imaging was recalibrated using APM catalogue stars, with a final uncertainty on the SN position as $\pm 0.7''$. A V-band image of NGC 4900 from the TNG, acquired 101 days after discovery with the OIG instrument (Pastorello et al. 2004), was utilised to provide a separate differential astrometric calibration. The SN position was located, using the TNG image, on the post-explosion ACS frames with a precision of 6 ACS/WFC pixels (the combined error of the “seeing” σ of the TNG image and the uncertainty in the transformation between the TNG and ACS images). The SN is not significantly recovered on the post-explosion WFPC2 images with limiting magnitudes $m_{F450W}(3\sigma) = 24.95$ and $m_{F814W}(3\sigma) = 24.33$. An object is recovered in the post-explosion ACS F435W and F555W images within the error circle of the differential astrometry from the TNG image. This object has magnitude $m_{F435W} = 26.19 \pm 0.20$ (4.3σ) and $m_{F555W} = 25.70 \pm 0.18$. This object does not appear significantly in the F814W image to a 3σ detection limit of $m_{F814W} = 26.18$. Figure 2 shows these magnitudes are consistent with the measured light curve of SN1999br of Pastorello et al. (2004). The post-explosion ACS and WFPC2 images were aligned with the pre-explosion WFPC2 frame. The SN location on the TNG, ACS and both the pre- and post-explosion WFPC2 images is shown as figure 3. The SN location falls on WF3 chip on the pre-explosion imaging with a positional uncertainty of 3 WF pixels. There is an indication of an object at the centre of the error circle, but it is just below the 3σ detection limit. Van Dyk et al. (2003) suggest an object $0.7''$ from the SN position, as determined from the post-explosion TNG image, and detected at 3.3σ is the likely progenitor. This object is indicated on figure 3b. The post-explosion ACS/WFC observations show two extended objects either side of the trans-

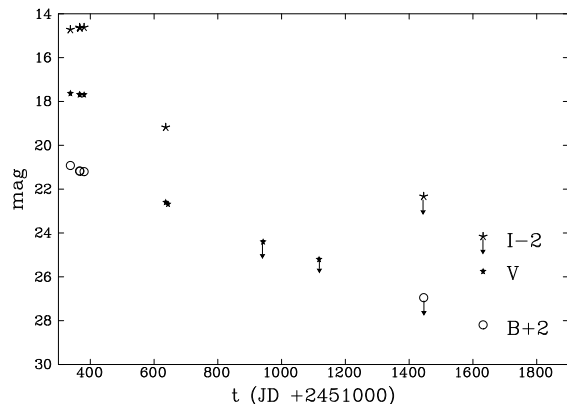


Figure 2. A figure showing the light curve of SN 1999br. Photometry of the early phases of the SN ($\text{JD} < 2452200$) is from Pastorello et al. (2004). Late time magnitudes and magnitude limits are from HST WFPC2 (GO 9042) and ACS (GO 9353) observations.

formed position of the centroid of this object on the pre-explosion frame. This suggests that the object imaged on the pre-explosion frame is merely the unresolved combination of these two features and not the progenitor. The limiting magnitude at the position of SN1999br on the pre-explosion image was determined to be $m_{F606W} = 24.91$. The reddening of nearby stars was determined to be $E(B - V) = 0 \pm 0.05$. NGC 4900 has an inclination of 16.5° and this reddening is consistent with a negligible contribution from internal extinction expected for such an almost face on spiral. We adopt, therefore, the NED quoted fore-ground extinction of $E(B - V) = 0.024$ towards NGC 4900. The limiting absolute magnitude for SN 1999br was, therefore, $M_{F606W} \geq -5.98$.

3.3 SN 1999ev

SN 1999ev was discovered by T. Boles (Hurst et al. 1999) on 1999 November 7.225. The position of the SN was $\alpha = 12^{\text{h}}19^{\text{m}}48^{\text{s}}.20$, $\delta = +29^{\circ}37'21''.7$ (Van Dyk et al. 2003), in the SBab galaxy of NGC 4274 ($v_{\text{vir}} = 1089\text{kms}^{-1}$). Garnavich et al. (1999) noted a strong $\text{H}\alpha$ P-Cygni profile consistent with a normal type II SN past maximum.

Figure 4. Pre- and post-explosion imaging of the site SN 1999ev in NGC 4274. (a) Pre-explosion WFPC2 F555W image. The progenitor was identified in this image, to a positional accuracy of 0.2 WF pixels on the pre-explosion image. The progenitor had magnitude $m_{F555W} = 24.64 \pm 0.17$, detected at 4.8σ . Stars A and B, suggested as candidates for the progenitor by Van Dyk et al. (2003), are not coincident with the SN recovered in the ACS imaging. (b) Post-explosion ACS/WFC F555W showing SN 1999ev, $m_V = 23.91 \pm 0.07$, and associated light echo feature not observed in the pre-explosion imaging. (c) Post-explosion ACS/WFC F814W imaging, the SN has magnitude $m_I = 23.35 \pm 0.08$.—see jpeg

Photometric observations⁶ of this SN show a plateau in the light curve and, hence, imply a II-P classification. The SN location had been imaged with a 296s F555W exposure on 1995 February 5 (program GO-5741, PI: J. Westphal). Post-explosion ACS WFC imaging, acquired on 2002 December 31, shows a new feature within the error circle of the SN position as determined from absolute astrometry. The pre- and post-explosion images are shown as figure 4. At the SN location on the pre-explosion frame WF2 chip, with an uncertainty of ± 0.2 WF pixels, is a star with $m_{F555W} = 24.64 \pm 0.17$, detected at a 4.8σ level. This is compared with the new object in the post-explosion ACS imaging with $m_V = 23.92 \pm 0.07$. Four stars fall within the absolute astrometric error circle on the pre-explosion imaging. The post-explosion imaging clearly identifies one of these stars, with sub-pixel accuracy, as the progenitor. Van Dyk et al. (2003) identified two stars, A and B, on the pre-explosion F555W frame and suggested these as candidates for the progenitors. In addition a separate star C, following the nomenclature of Van Dyk et al. (2003), is detected $\approx 0.2''$ from the progenitor in the pre-explosion image by both DAOPHOT (at a 3.3σ level) and HSTphot (Dolphin 2000b) photometry with magnitude $m_{F555W} = 25.03 \pm 0.24$. The post-explosion imaging allows for the confident rejection of stars A, B and C as the progenitor. A circular feature in the post-explosion imaging, unobserved in the pre-explosion images, is interpreted as a light echo from the SN (Liu et al. 2003). This is shown in figure 4b. The brightness of the SN in the B and I bands was: $m_B = 24.61 \pm 0.09$ and $m_I = 23.35 \pm 0.08$. The NED value for the foreground reddening towards NGC 4724 is $E(B - V) = 0.02$. The inclination of the galaxy of 71.8° , the paucity of observed stars in the vicinity of the SN and obvious dust lanes imaged in the post-explosion frames suggests a higher reddening is appropriate. Five stars, within $6''$ of the SN were utilised to determine a line of sight reddening of $E(B - V) = 0.15 \pm 0.05$. This implied an absolute magnitude for the progenitor of $M_{F555W} = -6.5 \pm 0.3$.

3.4 SN 2000ds

SN 2000ds was discovered by Puckett & Dowdle (2000) on 2000 October 10.4 in the galaxy of NGC 2768. The SN was classified as a type-Ib several months past maximum. Van Dyk et al. (2003) give the position of SN 2000ds as $\alpha = 9^{\text{h}}11^{\text{m}}36^{\text{s}}.28$, $\delta = +60^\circ 01' 43''.3$. Two epochs of pre-explosion observations were available in the HST archive. A single WFPC2 F555W observation was made on 1995 December 4, as part of program GO-5999 (PI: A. Phillips). This was an individual frame, without a companion frame for the removal of cosmic rays (CRs). The corresponding F814W

frame, composed of two CR-split observations, was only 320s. The longer F555W and F814W observations from 1998 (program GO-6587, PI: D. Richstone) were utilised to attempt to detect a progenitor. The post-explosion ACS/WFC images were astrometrically recalibrated, with 8 APM stars, with a precision of $\pm 0.23''$. The pre-explosion images from 1998 were aligned with the ACS images with a precision of $\pm 0.02''$. There is no discernible change between the pre-explosion and post-explosion images. This indicates that the SN has not been recovered in the late time images down to 3σ limiting magnitudes: $m_{F435W} = 27.55 \pm 0.32$, $m_{F555W} = 27.10 \pm 0.32$ and $m_{F814W} = 26.42 \pm 0.31$. The progenitor has not been detected in the pre-explosion images to limiting magnitudes of $m_{F555W} = 25.96$ and $m_{F814W} = 25.40$. The foreground reddening, quoted by NED towards NGC 2768, is $E(B - V) = 0.044$. The limiting absolute magnitudes of the progenitor were $M_{F555W} \geq -6.02$ and $M_{F814W} \geq -6.52$.

3.5 SN 2000ew

SN 2000ew was discovered by Puckett et al. (2000) on 2000 November 28.48 in the galaxy of NGC 3810, an Sc galaxy with an inclination of 47.8° . Dennefeld & Patris (2000) classified the SN as a type Ia, although Filippenko et al. (2000) later reclassified 2000ew as a type Ic SN. The latest estimate of the position of SN2000ew is $\alpha = 11^{\text{h}}40^{\text{m}}58^{\text{s}}.60$, $\delta = +11^\circ 27' 55''.8$ (Van Dyk et al. 2003). The SN location had been imaged with WFPC2 with the F606W filter, with an exposure time of 160s, on 1994 November 04 (program GO-5446, PI: G. Illingworth). This was 6.07 years prior to the discovery of SN2000ew. Two sets of post-explosion imaging were acquired with the WFPC2 and ACS/WFC instruments. WFPC2 images of the SN, 0.94 years after discovery, were acquired as part of program GO 9042 (PI: S. Smartt). Imaging of the SN, and host galaxy, was conducted in the F450W and F814W for 460s each. Observations of the SN, 1.58 years after discovery, were made with the ACS/WFC in F435W, F555W and F814W bands. The ACS/WFC images were astrometrically recalibrated with four stars from the APM catalogue. The SN position was located on the ACS images with a precision of $0.5''$. The pre- and post-explosion WFPC2 images were aligned with the ACS images, with a precision of $0.025''$ and $0.03''$ respectively. At the SN location the pre-explosion F606W frame and the post-explosion F555W ACS frame appear similar. In the post-explosion WFPC2 frames, however, a new object is seen and this is identified as the SN. We measure the brightness of this object in the F450W and F814W filters as $m_{F450W} = 22.19 \pm 0.08$ and $m_{F814W} = 20.94 \pm 0.03$. Nothing is detected at the SN location on the pre-explosion WFPC2 F606W frame, with a 3σ detection limit of $m_{F606W} = 24.6$. The reddening determined from the neighbouring stars is $E(B - V) = 0.01 \pm 0.03$. We adopt, therefore, the NED value $E(B - V) = 0.044$ towards

⁶ <http://www.rochesterastronomy.org/snimages/sn1999/sn1999ev.html> for the foreground reddening of $E(B - V) = 0.044$ towards

Figure 5. Pre- and post-explosion of the site of SN 2000ds in NGC 2768. (a) Pre-explosion F814W WFPC2 image of the site of SN 2000ds from 1995. Note the bright peak in the bottom right quadrant is a hot pixel. (b) Pre-explosion F555W WFPC2 images of the site of SN 2000ds from 1998. (c) Pre-explosion F814W WFPC2 image of the site of SN 2000ds from 1998. Note the bright peak in the bottom right quadrant is a hot pixel. (d) Post-explosion F435W ACS/WFC image of the site of SN 2000ds. Within the positional error circle nothing is recovered - suggesting both the progenitor and SN have not been observed in the pre- and post-explosion imaging. (e) Post-explosion F555W ACS/WFC image of the site of SN 2000ds. (f) Post-explosion F814W ACS/WFC image of the site of SN 2000ds. - see jpeg

Figure 6. Pre- and post-explosion imaging of the site SN 2000ew in the galaxy NGC 3810. (a) Pre-explosion WFPC2 F606W image, the SN fell on WF4 chip. At the SN location no object is seen. The WFPC2 images have been scaled, rotated and aligned with post-explosion ACS/WFC observations. (b) Post-explosion WFPC2 F814W image, with the SN on the WF3 chip, acquired as part of program HST GO 9042. (c) Post-explosion ACS/WFC F555W imaging with the fading SN.-see jpeg

to SN 2000ew. This implied a limiting absolute magnitude for the progenitor of $M_{F606W} \geq -6.42$.

3.6 SN 2001B

SN 2001B was discovered by Xu & Qiu (2001) in the Sc galaxy IC 391. While Matheson et al. (2001) classified SN 2001B as a type-Ia, Chornock & Filippenko (2001) later reclassified the SN as type Ib ~ 7 days post-maximum. Xu & Qiu (2001) reported a position for the SN of $\alpha = 4^{\text{h}}57^{\text{m}}19^{\text{s}}.24, \delta = +78^{\circ}11'16''.5$, whereas observations by Van Dyk et al. (2003) gave a position $\alpha = 4^{\text{h}}57^{\text{m}}19^{\text{s}}.24, \delta = +78^{\circ}11'16''.6$ with an uncertainty of $\pm 0.2''$. An individual 70s WFPC2 F555W image was available in the HST archive, acquired as part of program GO-5104 (PI: J. Westphal). This frame did not have a companion observation for the rejection of cosmic rays and, hence, in this case photometry was conducted with care to avoid inclusion of cosmic rays. This image was acquired prior to the "cool down" of the WFPC2 instrument, and the CTE appropriate for the epoch of acquisition of this frame has not been formalised (Dolphin 2000a). The post-explosion ACS/WFC F555W was astrometrically recalibrated using 8 APM stars with a precision of $\pm 0.34''$. The post-explosion images were aligned with the single pre-explosion frame to within $\pm 0.04''$. The SN location was determined to be on the WF3 chip on the pre-explosion frame. The pre- and post-explosion images are shown as figure 7. Van Dyk et al. (2003) identified star A, of figure 7, as the likely progenitor star. Inspection of the pre- and post-explosion frames shows, however, a new object on the post-explosion image within the astrometric error circle for the SN. No object is detected at this position on the pre-explosion image to a limit of $m_{F555W} = 24.301 \pm 0.145$. We identify this new object on the post-explosion frame as SN 2001B. The SN brightness in the ACS/WFC imaging was determined to be: $m_B = 23.52 \pm 0.02$, $m_V = 22.92 \pm 0.02$ and $m_I = 22.46 \pm 0.02$. The reddening towards SN 2001B was determined, using 68 stars within $6''$ of the SN, to be $E(B - V) = 0.102 \pm 0.030$. This is in agreement with NED value for the fore-ground reddening of $E(B - V) = 0.127$. The absolute magnitude for the progenitor on the F555W pre-explosion imaging was $M_{F555W} \geq -8.01$.

4 DISCUSSION

The detection limits of the progenitors, presented in §3, were interpreted as mass limits by placing the detection thresh-

olds on the Hertzsprung-Russell (HR) diagram. Mass limits were determined by comparing regions excluded by the detections limits, in which a progenitor would have been observed, with the progenitors predicted by stellar evolution models. Here we adopt the Geneva group non-rotating stellar evolution models of Lejeune & Schaerer (2001)⁷. Drilling & Landolt (2000) provide the standard colours of supergiants. These colours were transformed using the relations of Dolphin (2000a) to calculate the colour correction, as a function of supergiant spectral type, between the magnitudes in the WFPC2 photometric system and the corresponding Johnson-Cousins magnitude. The bolometric corrections, quoted by Drilling & Landolt (2000), were then utilised to calculate a luminosity for each spectral type. The colour and bolometric corrections and temperatures are given in table 4. In addition the Potsdam Wolf-Rayet (WR) Star Models synthetic spectra (Gräfener et al. 2002)⁸ were utilised to explore the luminosity behaviour of the detection threshold for WR stars. The synthetic spectra used are for an approximately solar abundance. These models are dependent, however, on two parameters: the effective temperature and the Transformed Radius, R_t . Bolometric corrections and colour corrections (between the Johnson V band and the WFPC2 F555W and F606W bands) were calculated from the synthetic spectra using the STSDAS *Synphot* package. Models were selected from the grid of synthetic spectra to form three groups with the maximum, median and minimum R_t for a given effective temperature. This takes into the account the spread in luminosities of WR stars, as parameterised by R_t . The results from these models are presented in table 5. The detection thresholds were converted to absolute magnitudes, using the extinctions determined here and the distance moduli quoted by LEDA (given in table 1).

$$m_{X;WFPC2} - M_{X;WFPC2} = 5 \log d - 5 + A_{X;WFPC2} \quad (5)$$

for the general filter X in the WFPC2 photometric system. The bolometric magnitudes, as a function of the effective temperatures for each spectral type, were then calculated from the absolute magnitudes using the formula:

$$M_{bol}(T_{eff}) = M_{X;WFPC2} + (M_{X;J-C} - M_{X;WFPC2}) + (M_V - M_{X;J-C}) + B.C. \quad (6)$$

⁷ <http://webast.ast.obs-mip.fr/stellar>

⁸ <http://www.astro.physik.uni-potsdam.de/~wrh/PoWR/powrgrid1.html>

Figure 7. Pre- and post-explosion imaging of the site of SN 2001B in IC 391. (a) Pre-explosion WFPC2 F555W imaging. The SN location was determined to be on the WF3 chip. Star A is observed in both the pre- and post-explosion images, although Van Dyk et al. (2003) identified it as the likely progenitor. (b) Post-explosion F555W imaging of SN 2001B. The SN was recovered in this late imaging. At the same location on the pre-explosion image no object is detected. (c) Post-explosion ACS/WFC F814W imaging of SN 2001B. - see jpeg

Table 4. A table showing the colours and bolometric corrections of supergiants, as given by Drilling & Landolt (2000). The corrections between magnitudes in the WFPC2 photometric system and the corresponding standard Johnson-Cousins magnitude were calculated using the updated transformations of Dolphin (2000a).

Sp	M(V)	B-V	U-B	V-R	R-I	T_{eff}	BC	V-I	B-F439W	B-F450W	V-F555W	V-F606W	I-F814W
O9	-6.5	-0.27	-1.13	-0.15	-0.32	32000	-3.18	-0.47	-0.007	-0.060	0.030	-0.108	0.035
B2	-6.4	-0.17	-0.93	-0.05	-0.15	17600	-1.58	-0.2	-0.003	-0.037	0.011	-0.041	0.013
B5	-6.2	-0.1	-0.72	0.02	-0.07	13600	-0.95	-0.05	-0.001	-0.021	0.003	-0.004	0.003
B8	-6.2	-0.03	-0.55	0.02	0	11100	-0.66	0.02	0.000	-0.005	-0.001	0.014	-0.001
A0	-6.3	-0.01	-0.38	0.03	0.05	9980	-0.41	0.08	0.000	0.000	-0.004	0.029	-0.005
A2	-6.5	0.03	-0.25	0.07	0.07	9380	-0.28	0.14	0.000	0.009	-0.007	0.045	-0.008
A5	-6.6	0.09	-0.08	0.12	0.13	8610	-0.13	0.25	0.000	0.023	-0.011	0.073	-0.014
F0	-6.6	0.17	0.15	0.21	0.2	7460	-0.01	0.41	-0.002	0.041	-0.017	0.115	-0.021
F2	-6.6	0.23	0.18	0.26	0.21	7030	0	0.47	-0.004	0.055	-0.018	0.131	-0.024
F5	-6.6	0.32	0.27	0.35	0.23	6370	-0.03	0.58	-0.008	0.075	-0.021	0.160	-0.028
F8	-6.5	0.56	0.41	0.45	0.27	5750	-0.09	0.72	-0.026	0.130	-0.023	0.198	-0.032
G0	-6.4	0.76	0.52	0.51	0.33	5370	-0.15	0.84	-0.049	0.175	-0.025	0.231	-0.034
G2	-6.3	0.87	0.63	0.58	0.4	5190	-0.21	0.98	-0.064	0.200	-0.025	0.269	-0.037
G5	-6.2	1.02	0.83	0.67	0.44	4930	-0.33	1.11	-0.088	0.233	-0.024	0.306	-0.038
G8	-6.1	1.14	1.07	0.69	0.46	4700	-0.42	1.15	-0.111	0.260	-0.024	0.317	-0.038
K0	-6	1.25	1.17	0.76	0.48	4550	-0.5	1.24	-0.134	0.285	-0.023	0.342	-0.038
K2	-5.9	1.36	1.32	0.85	0.55	4310	-0.61	1.4	-0.159	0.309	-0.020	0.388	-0.038
K5	-5.8	1.6	1.8	1.2	0.9	3990	-1.01	2.1	-0.220	0.362	0.010	0.567	-0.020
M0	-5.6	1.67	1.9	1.23	0.94	3620	-1.29	2.17	-0.240	0.378	0.014	0.569	-0.017
M2	-5.6	1.71	1.95	1.34	1.1	3370	-1.62	2.44	-0.252	0.387	0.034	0.583	-0.002
M5	-5.6	1.8	1.6	2.18	1.96	2880	-3.47	4.14	-0.280	0.406	0.247	0.890	0.172

Where $M_{X;J-C} - M_{X;WFPC2}$ is the colour correction for the general passband X in the WFPC2 photometric system and the corresponding passband in the Johnson-Cousins photometric system. The luminosity was calculated using the standard formula:

$$\log(L(T_{\text{eff}})/L_{\odot}) = \frac{M_{\text{bol}} - 4.74}{-2.5} \quad (7)$$

In this way the luminosity limit was calculated for a range of temperatures over all supergiant spectral types. The limiting luminosity describes an ‘‘arc’’ across the HR diagram depending on the colour and temperature (and hence the bolometric correction). A progenitor star with a luminosity greater than the determined limit would have been observed in the pre-explosion frames. In addition the stellar populations surrounding the progenitors were examined. The approximate ages of these stars were determined by examining the locus of these stars on colour-magnitude diagrams. Isochrones, produced by the Geneva stellar evolution group (Lejeune & Schaerer 2001), were overlaid on these diagrams to determine the ages. Metallicities were estimated, in the broad groups of SMC, LMC, Solar and twice Solar, by considering the relationship of Pilyugin et al. (2004) and the absolute magnitudes of the host galaxies quoted in LEDA. In addition the metallicity gradient of NGC 2403 (Garnett et al. 1997) was adopted to estimate the metallicity at the radii of the SNe.

4.1 SN 1999an

The detection threshold $M_{F606W} \geq -7.5 \pm 0.3$ for the progenitor of SN 1999an was plotted on an HR diagram. The metallicity was assumed to be solar. The determination of the appropriate metallicity for SN 1999an and its progenitor was hampered by the high inclination of the host galaxy and the line of sight proximity of the SN to the centre of the galaxy. An HR diagram, showing the region excluded by the pre-explosion imaging and the non-detection of the progenitor, is shown as figure 8. A red supergiant progenitor, with an initial mass $> 20M_{\odot}$, would have been detected in the pre-explosion F606W image. The age of the surrounding stellar population, see figure 9, is ≈ 14 Myr. This is consistent the approximate life time of stars with $M_{ZAMS} = 15 - 20M_{\odot}$. The inclination of IC 755 complicates the age determination procedure by probing various radii of the host galaxy, as well as reddening and ages in nearby lines of sight. This is responsible for the apparent spread in the observed colour-magnitude diagram for stars in IC 755. This mass limit is consistent with the mass limits determined for type II-P SNe (Smartt et al. 2003).

4.2 SN 1999br

The metallicity at the position of SN1999br, in NGC 4900, was estimated as approximately solar. Exclusion zones were plotted on the HR diagram for the limiting detection mag-

Table 5. The colour corrections, between the WFPC2 and Johnson-Cousins photometric systems, and bolometric corrections for a range of WR star parameters calculated from the synthetic spectra of Gräfener et al. (2002). The table is separated by the maximum, median and minimum Transformed Radii R_t at each effective temperature.

Minimum					
Temp (K)	Model No.	$\log R_t$	V-F555W	V-F606W	<i>B.C.</i>
70800	10-21	0	0.053	0.103	-2.737
63100	09-20	0.1	0.049	0.106	-2.700
56200	08-19	0.2	0.044	0.089	-2.667
50100	07-18	0.3	0.040	0.079	-2.632
44700	06-17	0.4	0.033	0.070	-2.585
39800	05-16	0.5	0.028	0.057	-2.527
35500	04-15	0.8	0.024	0.052	-2.441
31600	03-10	1.1	0.024	0.008	-2.751
Median					
Temp (K)	Model No.	$\log R_t$	V-F555W	V-F606W	<i>B.C.</i>
177800	18-20	0.1	0.165	0.068	-5.974
158500	17-19	0.2	0.191	0.075	-5.850
141300	16-18	0.3	0.195	0.070	-5.739
125900	15-17	0.4	0.195	0.061	-5.642
100000	13-16	0.5	0.171	0.055	-5.192
89100	12-15	0.6	0.166	0.056	-5.133
70800	10-13	0.8	0.121	0.033	-4.796
63100	09-12	0.9	0.104	0.020	-4.622
56200	08-11	1.0	0.102	0.020	-4.350
50100	07-10	1.1	0.099	0.088	-4.083
44700	06-09	1.2	0.096	0.154	-3.788
39800	05-08	1.3	0.051	0.103	-3.509
35500	04-05	1.6	0.028	0.018	-3.202
Maximum					
Temp (K)	Model No.	$\log R_t$	V-F555W	V-F606W	<i>B.C.</i>
199500	19-16	0.5	0.064	0.012	-7.818
177800	18-13	0.8	0.046	-0.025	-7.898
158500	17-12	0.9	0.043	-0.033	-7.561
141300	16-11	1.0	0.041	-0.038	-7.227
125900	15-10	1.1	0.041	-0.046	-7.016
112200	14-09	1.2	0.039	-0.041	-6.633
100000	13-08	1.3	0.044	-0.042	-6.406
79400	11-06	1.5	0.040	-0.049	-5.804
70800	10-05	1.6	0.034	-0.052	-5.431
56200	08-04	1.7	0.032	-0.045	-4.707

nitude of the pre-explosion F606W image. These are shown as figures 10 and 11. A useful upper mass limit cannot be placed on the progenitor with the F606W observation and considering a WR star progenitor. Pastorello et al. (2004) find, from observations of the light curves, a long plateau and a low tail luminosity indicates a massive H envelope and low Ni production. The long light curve plateau is consistent with a red supergiant progenitor, which the F606W observation limits to $M_{ZAMS} \leq 12M_{\odot}$. Turatto et al. (1998) estimate a progenitor mass of $26M_{\odot}$ for the similarly faint SN 1997D. In this scenario the low luminosity of the SN arises from the fall back of Ni onto a newly formed black

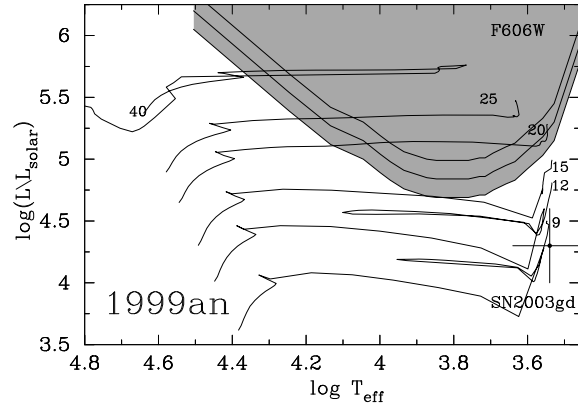


Figure 8. An HR diagram showing the luminosity and temperature region (in grey) where stars would have been detected in pre-explosion imaging. The progenitor of SN 1999an is not detected to an absolute magnitude of $M_{F606W} \geq -7.5 \pm 0.3$ (or $\Delta L = \pm 0.12$). The detection region shows that the progenitor of SN 1999an had a mass $M_{ZAMS} < 20M_{\odot}$ for it not to have been detected in the HST WFPC2 pre-explosion F606W imaging.

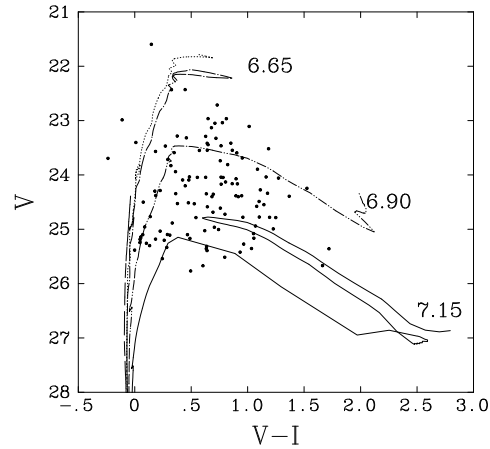


Figure 9. Colour-magnitude diagram showing the locus of stars in the vicinity of the progenitor of SN 1999an. Overlaid are solar metallicity isochrones shifted to the distance, extinction and reddening determined for the progenitor in IC 755. The age of the stellar population is $\log(\text{Age}/\text{years}) = 7.15 \pm 0.25$. This age is consistent with the expected life time for stars with $M_{ZAMS} = 15 - 20M_{\odot}$. The large spread in apparent ages is due to the varying depth, reddening and ages being probed in nearby lines of sight because of the inclination of IC 755.

hole. Models of Heger et al. (2003) suggests this happens for stars with $30M_{\odot} \leq M_{ZAMS} \leq 40M_{\odot}$. Alternatively Chugai & Utrobin (2000) suggest a low mass progenitor, $8 - 12M_{\odot}$, for SN 1997D. The latter estimate is a similar mass to the observed progenitor of the normal type II-P SNe 1999em, 1999gi, 2001du and 2003gd (Smartt et al. 2004). Zampieri et al. (2003) and Pastorello et al. (2004) estimate, from models of photometric and spectroscopic observations of SN 1999br, an ejected envelope mass of $14 - 19M_{\odot}$ from an intermediate mass progenitor of mass $\geq 16M_{\odot}$.

The pre-explosion observation, however, rules out a bright red supergiant progenitor for SN 1999br, as has been pro-

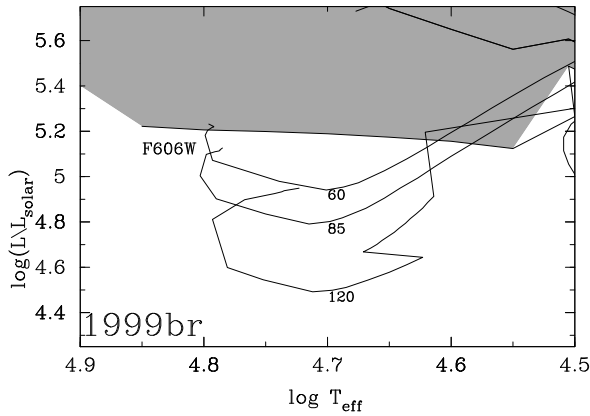


Figure 10. A figure showing the detection limit of the F606W pre-explosion observation, at the location of SN 1999br, on the blue side of the HR diagram. Overlaid are solar metallicity stellar evolution tracks for $M_{ZAMS} = 60, 85$ and $120M_{\odot}$.

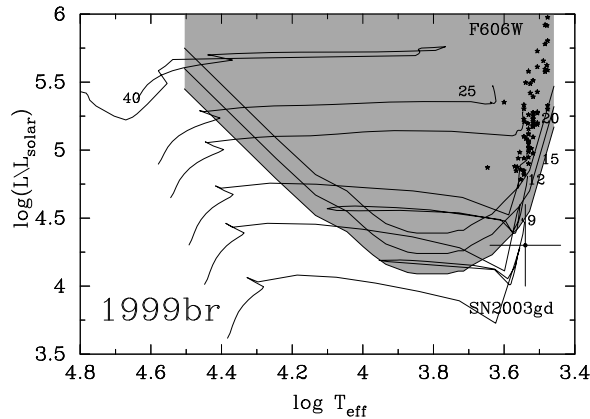


Figure 11. A figure showing the detection limit of the F606W pre-explosion observation, of the location of SN 1999br, on the red side of the HR diagram. Stars with $12M_{\odot} < M_{ZAMS} < 25M_{\odot}$ are excluded as progenitors in a single star scenario. The locus of observed red supergiants, in the LMC (Massey & Olsen 2003), is shown by the starred points. The brightest of these red supergiants would have been detected in the pre-explosion imaging.

posed for SN 1997D. The locus of observed red supergiants, in the LMC, on the HR diagram is shown on figure 11. A very massive red supergiant progenitor would have been significantly detected on the pre-explosion F606W image.

The pre-explosion observation supports the hypothesis of Chugai & Utrobin (2000) that such faint SNe arise from low mass progenitors. The simultaneous production of both faint and normal type II-P SNe from the same range of initial masses $M_{ZAMS} = 8 - 12M_{\odot}$ is not unexpected. The evolution of stars in this range is particularly sensitive to initial mass as it includes the transition between electron-degenerate and non-degenerate stellar cores and slight differences in initial mass will lead to different SN outcomes (Nomoto 1984; Eldridge & Tout 2004). SNe originating from the core-collapse of degenerate cores are predicted to produce little Ni due to the presence of steep density gradients at the edges of the cores. This leads to only small

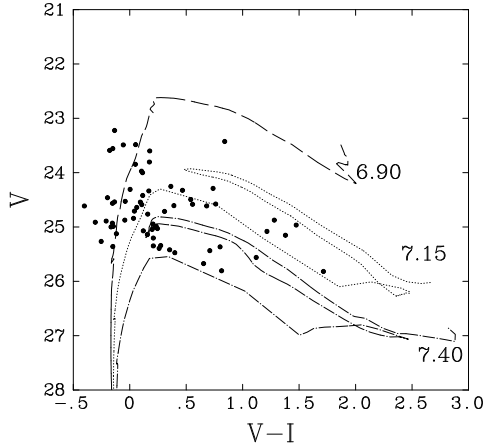


Figure 12. A V, V-I colour magnitude diagram for stars within $6''$ of the site of SN 1999br. The surrounding population defines a tight locus on the diagram. Overlaid are solar metallicity isochrones, corrected for the distance of and reddening towards NGC 4900. The surrounding stellar population has an age of $\log(\text{Age}/\text{years}) = 7.15 \pm 0.25$. This age is consistent with the lifetime of a star with $M_{ZAMS} \sim 9 - 20M_{\odot}$.

amounts of material being sufficiently heated to produce Ni (Heger et al. 2003). The age of the progenitor was estimated from the approximate ages of nearby stars (within $6''$ of the SN location) in NGC 4900. The locus of these stars on the V, V-I colour magnitude diagram is shown as figure 12. The age was determined as $\log(\text{Age}/\text{years}) = 7.15 \pm 0.25$, which is consistent with a progenitor of initial mass $\sim 9 - 20M_{\odot}$.

4.3 SN 1999ev

The brightness of the identified progenitor star for SN1999ev was plotted on an HR diagram, shown as figure 13. The proximity of the SN to the centre of NGC 4724 suggests that the appropriate metallicity for the progenitor of SN 1999ev is closer to twice solar. A study of the metallicity of NGC 4274 and its gradient has not been conducted. Because the progenitor star was only observed in a single filter the absence of any colour information gives a degeneracy in temperature. The allowed region on the HR diagram for the progenitor of SN encompasses the red supergiant end points for stars with $15 < M_{ZAMS} < 18M_{\odot}$. The photometry of the stars surrounding the progenitor is shown of the colour-magnitude diagram figure 14. The age of these stars, $\log(\text{Age}/\text{years}) = 7.15 \pm 0.25$, is consistent with the theoretically predicted life times for stars with $M_{ZAMS} = 15 - 20M_{\odot}$ (6.95 and 7.1 respectively). This mass is higher than both the determined progenitor mass for SN 2003gd and the mass limits for a number of normal type II-P SNe by Smartt et al. (2003) ($M_{ZAMS} < 15M_{\odot}$).

4.4 SN 2000ds

The two colour detection limits from the pre-explosion F555W and F814W were simultaneously utilised to place a mass limit on the progenitor of SN 2000ds. The classification of the host galaxy makes the determination of the appropriate metallicity and the interpretation of the progenitor dif-

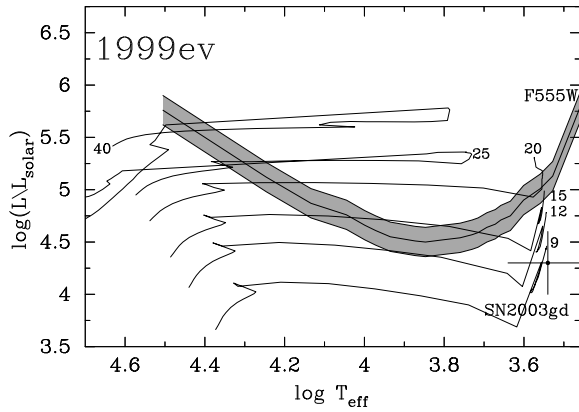


Figure 13. An HR diagram showing the locus of allowed luminosities for the progenitor of SN 1999ev, given an absolute magnitude of $M_{F555W} = -6.5$. The thick line shows the median luminosity, at a given temperature, for that absolute magnitude. The two thin lines show the upper and lower boundaries of the luminosity given the uncertainty in the absolute magnitude, the distance to the host galaxy and the reddening along the line of sight ($\Delta L = \pm 0.11$). The observed progenitor, assuming a red supergiant, had mass $M_{ZAMS} = 15 - 18 M_{\odot}$.

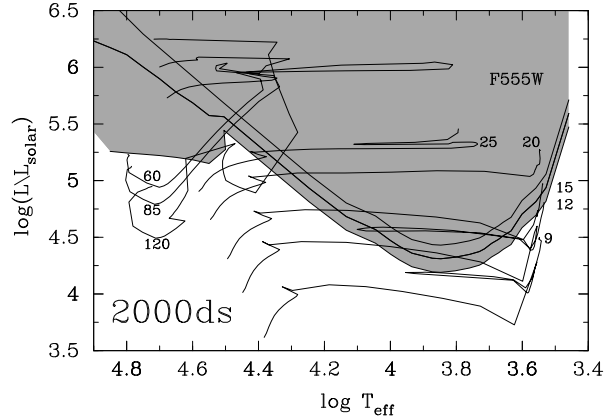


Figure 15. A figure showing the detection threshold of pre-explosion F555W WFPC2 imaging at the site of SN 2000ds. Over plotted are solar metallicity stellar evolution tracks. The end of the $40 M_{\odot}$ track lies at the same position as the end of the $85 M_{\odot}$ track. The F555W detection limit excludes stars with $12 M_{\odot} < M_{ZAMS} < 25 M_{\odot}$.

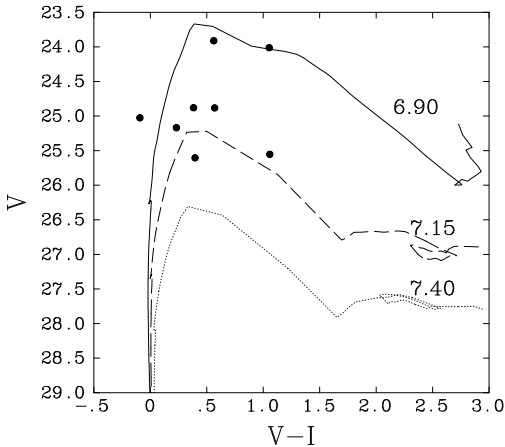


Figure 14. Colour-magnitude diagram showing the locus of stars in the vicinity of the progenitor of SN 1999ev. Overlaid are twice-solar metallicity isochrones shifted to the distance, extinction and reddening determined for the progenitor. The stellar population is clustered around the isochrones for $\log(\text{Age}/\text{years}) = 7.15 \pm 0.25$. This age is consistent with the expected life time for stars with $M_{ZAMS} = 15 - 20 M_{\odot}$.

difficult. van den Bergh et al. (2003) classify the host galaxy NGC 2768 as E3/Sa and the inclination for the galaxy, quoted by LEDA, is unclear. In this case, therefore, a solar metallicity has been adopted. The detection thresholds from the pre-explosion F555W and F814W imaging are shown as figures 15 and 16 respectively. The combined detection limit of both sets of imaging, shown as figure 17 exclude a red supergiant progenitor down to $M_{ZAMS} \approx 7 M_{\odot}$. A massive blue progenitor cannot be excluded. If NGC 2768 is an E3 galaxy a single massive progenitor is unlikely and the core-collapse of a blue low mass progenitor in a binary would be a plausible progenitor scenario.

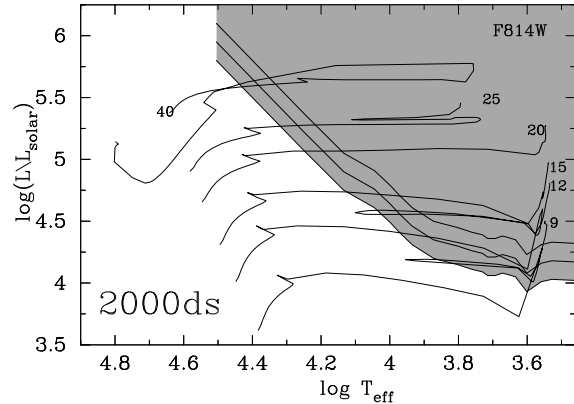


Figure 16. A figure showing the detection threshold of pre-explosion F814W WFPC2 imaging of the site of SN 2000ds. Over plotted are solar metallicity stellar evolution tracks. The F814W detection limit excludes a red supergiant progenitor with $M_{ZAMS} > 7 M_{\odot}$.

4.5 SN 2000ew

Given the proximity of the site of SN 2000ew to the centre of the host galaxy NGC 3810 the metallicity has been estimated as twice-solar. The detection threshold for the progenitor of SN 2000ew, from pre-explosion F606W imaging, is shown as figure 18. A massive Wolf-Rayet progenitor ($M_{ZAMS} > 25 M_{\odot}$) cannot be explicitly excluded from the pre-explosion imaging. The age of stars in the locality of SN 2000ew, shown as figure 19, was determined to be $\log(\text{Age}) = 6.9 \pm 0.25$. This is consistent with the lifetime of stars with $12 M_{\odot} < M_{ZAMS} < 40 M_{\odot}$. Post-explosion ACS imaging of SN 2000ew was useful to show not only the location of the SN but, by comparison with post-explosion WFPC2 imaging acquired at an early epoch, the SN fading.

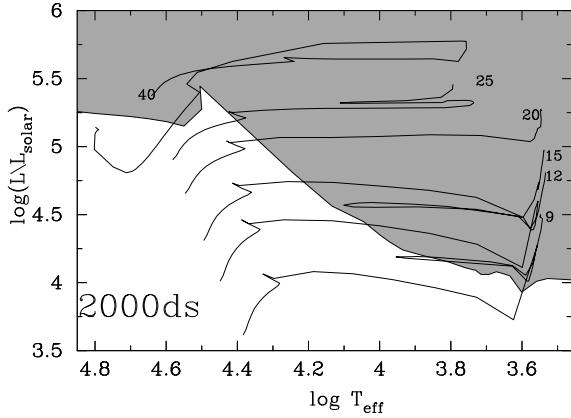


Figure 17. An HR diagram simultaneously showing the detection thresholds from all pre-explosion imaging of SN 2000ds. A red progenitor is excluded by the deep pre-explosion F814W imaging.

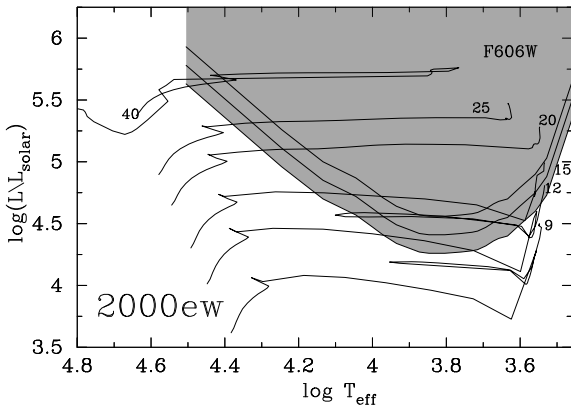


Figure 18. An HR diagram showing the detection threshold for pre-explosion F606W image. A red supergiant progenitor with an initial mass $> 12M_{\odot}$ would have been detected in the pre-explosion imaging. Overlaid are stellar evolution tracks for $Z = Z_{\odot}$.

4.6 SN 2001B

The detection limit for the F555W pre-explosion imaging is shown as figure 20. Solar metallicity stellar evolution tracks were utilised to estimate the mass limits for the progenitor. The mass limit for a red supergiant progenitor is $M_{ZAMS} < 25M_{\odot}$. Similarly to SN 2000ew a single blue massive progenitor ($> 25M_{\odot}$) is also permitted. A WR progenitor is favoured given the type Ib classification.

4.7 General Discussion

The mass limits for the progenitors of the SNe discussed here are summarised in table 6. The mass limits are presented on a SN populations diagram (Heger et al. 2003), shown as figure 22. Smartt et al. (2003) present masses or mass limits for SN progenitors, prior to SN 2003gd, with pre-explosion imaging. The interpretation of these results is complicated by the different progenitor scenarios which give rise to each CCSN type.

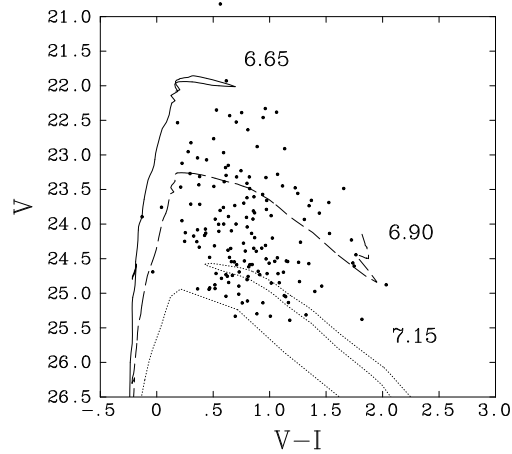


Figure 19. Colour-magnitude diagram showing the locus of stars within $6''$ of SN 2000ew. Overlaid are twice solar metallicity isochrones, corrected for the distance and reddening to the host galaxy NGC 3810. The age of the stellar population is $\log(\text{Age}/\text{years}) = 6.9 \pm 0.25$, approximately consistent with a progenitor $12M_{\odot} < M_{ZAMS} < 40M_{\odot}$.

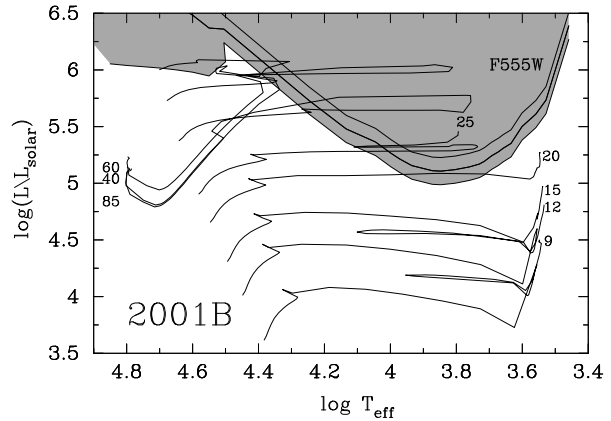


Figure 20. An HR diagram showing the detection threshold for pre-explosion F555W imaging of the location of SN 2001B. The detection threshold allows a single red progenitor up to a mass of $M_{ZAMS} = 22M_{\odot}$. A blue Wolf-Rayet progenitor is not excluded.

Table 6. A table summarising the mass limits for the progenitors of SNe 1999an, 1999br, 1999ev, 2000ds, 2000ew and 2001B, as derived from pre-explosion HST WFPC2 imaging.

SN	Type	Mass Limit
1999an	II(P)	$M_{ZAMS} \leq 20M_{\odot}$
1999br	IIpec	$M_{ZAMS} \leq 12M_{\odot}$
1999ev	II(P)	$15 \leq M_{ZAMS} \leq 18M_{\odot}$
2000ds	Ib	$M_{ZAMS} > 25M_{\odot}$ or binary?
2000ew	Ic	$M_{ZAMS} > 25M_{\odot}$ (WR?)
2001B	Ib	$M_{ZAMS} > 25M_{\odot}$ (WR?)

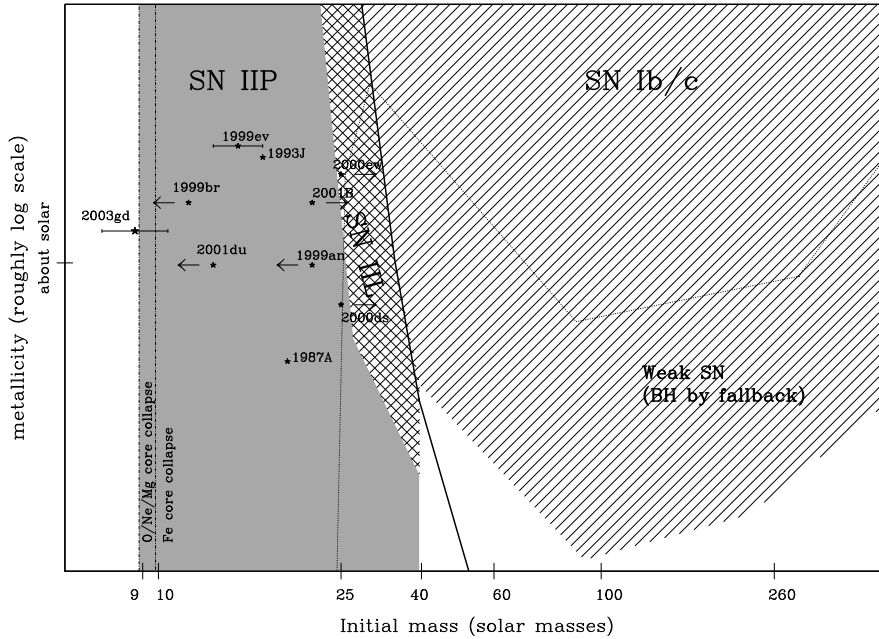


Figure 22. A SN Populations diagram (Heger et al. 2003) showing the locus of the 6 progenitors studied here: 1999an, 1999br, 1999ev, 2000ds, 2000ew and 2001B. In addition the positions of the three SNe with known progenitors, 1987A, 1993J and 2003gd, are shown. The upper mass limit for the progenitor of SN 2001du illustrates the expected mass regime for common type II-P SNe. Each of the mass limits is consistent with the predicted progenitors for each of the SN types. Approximate metallicities have been adopted to place the progenitors on the diagram.

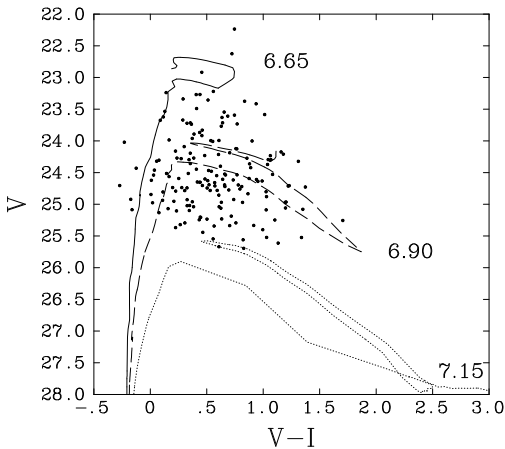


Figure 21. A colour-magnitude diagram showing the locus of stars within $6''$ of SN 2001B. Overlaid are solar metallicity isochrones, corrected for the distance and reddening to the host galaxy IC 391. The age of the stellar population is $\log(\text{Age}/\text{years}) = 6.9 \pm 0.25$, approximately consistent with a progenitor $12M_{\odot} < M_{ZAMS} < 25M_{\odot}$.

The progenitor mass limits for the type II SNe (1999an, 1999br and 1999ev) are consistent with the previously determined mass limits for the type II-P SNe 1999em, 1999gi and 2001du (Smartt et al. 2003). It has been assumed that the progenitors of these SNe arise from red supergiant progenitors. Only in the case of SN 1999br, however, has a sub-

type been firmly established by long term photometric and spectroscopic monitoring (Pastorello et al. 2004). Reported photometry from amateur observers suggests that 1999an and 1999ev were also type IIP SNe. The upper mass limit for the progenitor of SN 1999an does not place a tight constraint on the mass range of progenitors that give rise to type II-P SNe. Previous estimates of the mass of the progenitors of these SNe (Smartt et al. 2003, 2004) place the mass in the range $8 \leq M_{ZAMS} \leq 15M_{\odot}$. The observed mass for the progenitor of SN 1999ev shows that type II-P SNe also arise from higher mass progenitors. This would be inconsistent with the models of Zampieri et al. (2003), for SN 1999br, if all such high mass progenitors are predicted to only give rise to faint SNe.

It has not been possible to place constraining limits on the progenitors of the type I SNe (2000ds, 2000ew and 2001B) from their pre-explosion imaging. For SNe 2000ew and 2001B the observations do not explicitly exclude a red progenitor. The pre-explosion imaging for 2000ds, in both the V and I bands, allows the possibility of a red progenitor to be considered and ultimately excluded. In a single star star scenario the progenitor would be star with $M_{ZAMS} > 25M_{\odot}$ in the WR phase (Izzard et al. 2004). The available pre-explosion F555W/F606W imaging is biased against the discovery of the hot, low luminosity WR stars, which would require long U and B band imaging to detect. In addition Izzard et al. (2004) describe the evolution of a low mass progenitor ($10 - 20M_{\odot}$) in binaries, stripped by a companion, in the form of a naked helium star. These would

have temperature $\sim 100,000K$ and would thus appear on the blue side of the HR diagram and would be similarly undetectable. The location of SN 2000ds, in an S0 galaxy or earlier, strongly suggests that this SN arose in a binary system. The pre-explosion imaging does not permit the discrimination between SNe arising from the high or low mass progenitor scenarios. The pre-explosion imaging does, however, permit the exclusion of stars on the high mass end of the red/yellow supergiant branch at $M_{ZAMS} \approx 25M_{\odot}$.

The nature of the progenitor just prior to explosion depends on processes such as convection, mass loss, rotation and metallicity at various stages of the stars' lives. The way these processes are implemented in the stellar evolution codes affects the predicted properties of the progenitors. Eldridge & Tout (2004) notes the inclusion of convective overshooting reduces the initial mass for the progenitor of SN 2003gd from 10 to $8M_{\odot}$. The utilisation of different mass loss prescriptions also causes differences between the predictions of different stellar evolution codes. The non-rotating Geneva stellar evolution code, used here, predicts that increasingly more massive stars (up to $25M_{\odot}$) should give rise to hotter, more luminous progenitors culminating in a yellow supergiant (YSG) progenitor. More massive stars will undergo a WR phase and will explode as type Ibc SNe. Eldridge & Tout (2004) find that, in the mass range $8 - 25M_{\odot}$, more massive red supergiant progenitors are increasingly more luminous, but slightly cooler. This is consistent with observations of LMC supergiants by Massey & Olsen (2003). The use of different mass loss prescriptions causes the IIP \rightarrow IIL \rightarrow IIb \rightarrow Ibc transition zone to move (see figure 22; Heger et al. 2003; Eldridge & Tout 2004). Hirschi et al. (2004) shows that the inclusion of rotation can lead to YSG, having undergone a blue loop, and blue supergiant (BSG) progenitors for stars with $M_{ZAMS} \approx 20M_{\odot}$ with rotational velocities of 300kms^{-1} . Pre-explosion observations with the F555W and F606W filters with WFPC2 are not sensitive to BSGs, but do exclude YSG progenitors for this sample of SNe. Direct detections of the progenitors of CCSNe will allow the different approaches of different stellar evolution models to be tested.

Purpose acquired post-explosion imaging of these SNe has permitted, in this study, the confident identifications of some of the SNe on pre-explosion frames. In the specific cases of SNe 1999br, 1999ev, 2000ew and 2001B this has enabled the correct identification of the progenitor position in crowded regions on the pre-explosion imaging and the exclusion of nearby stars as candidates for the progenitor (Van Dyk et al. 2003). In two cases, however, the SN was not recovered on the post-explosion imaging due to a large intervening period between the SN explosion and the ACS/WFC observations. Target of Opportunity override programs with HST will be utilised to acquire the necessary post-explosion imaging for future nearby CCSNe to provide confident identification of progenitors. The analysis of the progenitors of the objects studied here was limited by the depth and spectral coverage of the pre-explosion data available (generally short single filter images). Programs to acquire deep multi-wavelength imaging of nearby galaxies are currently underway, to improve the chances of detecting the progenitors and analysing their parameters.

5 CONCLUSIONS

We have presented mass estimates for six progenitors of CCSNe, from pre-explosion HST WFPC2 observations. The identification of the progenitors on the pre-explosion imaging was aided by high resolution post-explosion imaging with the HST ACS/WFC. SNe 1999br, 1999ev, 2000ew and 2001B were recovered in the HST post-explosion imaging. The progenitor for SN 1999ev was confidently identified on F555W pre-explosion imaging, consistent with the progenitor expected for a star with $M_{ZAMS} = 15 - 18M_{\odot}$. The progenitors for 1999an, 1999br, 2000ds, 2000ew and 2001B were below the 3σ detection thresholds of their pre-explosion imaging. The mass limits determined for the three IIP SNe (1999an, 1999br and 1999ev) are consistent with mass limits previously placed on SNe of this type and SN 2003gd, for which a progenitor was identified. The observed progenitor of SN 1999ev shows that high mass stars ($> 15M_{\odot}$) can give rise to normal type II-P SNe. Our study of SN 1999br has shown that this faint SN arose from a low mass progenitor, in the same initial mass range as the progenitor of SN 2003gd, rather than a high mass progenitor. This does not exclude the possibility of high mass progenitors, such as that of SN 1999ev, giving rise to peculiarly faint SNe. The mass limits for the progenitors of the type I CCSNe (2000ds, 2000ew and 2001B) do not disagree with the predictions that these should arise from very high temperature WR stars. In this study the mass limits determined have assumed a single progenitor scenario. In the case of SN 2000ds a binary progenitor is much more likely, being consistent with both the lack of detection of the progenitor in the red and the age of the stellar population of NGC 2768. The detection of a blue WR progenitor, in multiple pass bands, will be an important test of stellar evolution predictions and will be significant for the understanding of such phenomenon as GRBs. The results presented here do, in general, concur with those of Van Dyk et al. (2003). We argue, however, that post-explosion imaging of SNe 1999br, 1999ev 2000ew and 2001B allows for the confident exclusion of nearby objects as the progenitors of these SNe. This demonstrates the importance of high resolution follow-up post-explosion imaging for this type of study.

ACKNOWLEDGMENTS

JRM acknowledges financial support, in the form of a studentship, from PPARC. This paper makes use of data obtained from the APM online sky catalogues which are maintained by the Cambridge Astronomical Survey Unit at the Institute of Astronomy, Cambridge. Based on observations made with the NASA/ESA Hubble Space Telescope, obtained from the data archive at the Space Telescope Science Institute. STScI is operated by the Association of Universities for Research in Astronomy, Inc. under NASA contract NAS 5-26555. This research has made use of the NASA/IPAC Extragalactic Database (NED) which is operated by the Jet Propulsion Laboratory, California Institute of Technology, under contract with the National Aeronautics and Space Administration. JRM and SJS thank A. Pastorello, for the provision of TNG data, W.-R. Hamann, for the provision of the Potsdam Wolf-Rayet Models, and

A. Mackey, J. Eldridge and N. Trentham for useful discussion.

References

- Aldering G., Humphreys R. M., Richmond M., 1994, *AJ*, 107, 662
- Branch D., Livio M., Yungelson L. R., Boffi F. R., Baron E., 1995, *PASP*, 107, 1019
- Cardelli J. A., Clayton G. C., Mathis J. S., 1989, *ApJ*, 345, 245
- Chornock R., Filippenko A. V., 2001, *IAUC*, 7577, 2
- Chugai N. N., Utrobin V. P., 2000, *A&A*, 354, 557
- Cox C., Mack J., 2004, Instrument Science Report ACS 2002-002, ACS Distortion derived from RAS-HOMS Measurements. Space Telescope Science Institute
- Dennefeld M., Patris J., 2000, *IAUC*, 7532, 3
- Dolphin A. E., 2000a, *PASP*, 112, 1397
- Dolphin A. E., 2000b, *PASP*, 112, 1383
- Drilling J. S., Landolt A. U., 2000, in Cox A. N., ed., , *Allen's Astrophysical Quantities*, 4 edn, AIP, New York
- Eldridge J. J., Tout C. A., 2004, *MNRAS*, 353, 87
- Filippenko A. V., 1997, *ARAA*, 35, 309
- Filippenko A. V., Chornock R., Modjaz M., 2000, *IAUC*, 7547, 2
- Filippenko A. V., Stern D., Reuland M., 1999, *IAUC*, 7143, 2
- Garnavich P., Jha S., Challis P., Kirshner R., Calkins M., 1999, *IAUC*, 7143, 1
- Garnavich P., Jha S., Kirshner R., Challis P., 1999, *IAUC*, 7306, 1
- Garnett D. R., Shields G. A., Skillman E. D., Sagan S. P., Dufour R. J., 1997, *ApJ*, 489, 63
- Gilmozzi R., Cassatella A., Clavel J., Gonzalez R., Fransson C., 1987, *Nature*, 328, 318
- Gräfener G., Koesterke L., Hamann W.-R., 2002, *A&A*, 387, 244
- Hamuy M., 2003, *ApJ*, 582, 905
- Hamuy M., Pinto P. A., 2002, *ApJL*, 566, L63
- Heger A., Fryer C. L., Woosley S. E., Langer N., Hartmann D. H., 2003, *ApJ*, 591, 288
- Hirschi R., Meynet G., Maeder A., 2004, *A&A*, 425, 649
- Holtzman J. A., Burrows C. J., Casertano S., Hester J. J., Trauger J. T., Watson A. M., Worthey G., 1995, *PASP*, 107, 1065
- Holtzman J. A., Hester J. J., Casertano S., et al. 1995, *PASP*, 107, 156
- Hurst G. M., Boles T., Armstrong M., Schwartz M., 1999, *IAUC*, 7306, 1
- Irwin M., McMahon R., 1992, in IAU Commission on Instruments APM Northern Sky Catalogue. pp 31–+
- Izzard R. G., Ramirez-Ruiz E., Tout C. A., 2004, *MNRAS*, 348, 1215
- King J. Y., 1999, *IAUC*, 7141, 1
- Krist J., Hook R., 2004, *The Tiny Tim User's Guide*. 6.3 edn
- Lütticke R., Dettmar R.-J., Pohlen M., 2000, *A&A*, 362, 435
- Lejeune T., Schaerer D., 2001, *A&A*, 366, 538
- Lentz E. J., Baron E., Lundqvist P., et al. 2001, *ApJ*, 547, 406
- Liu J., Bregman J. N., Seitzer P., 2003, *ApJ*, 582, 919
- Massey P., Olsen K. A. G., 2003, *AJ*, 126, 2867
- Matheson T., Jha S., Challis P., Kirshner R., Calkins M., 2001, *IAUC*, 7563, 2
- Maund J. R., Smartt S. J., Kudritzki R. P., Podsiadlowski P., Gilmore G. F., 2004, *Nature*, 427, 129
- Monet D. G., Levine S. E., Canzian B., et al. 2003, *AJ*, 125, 984
- Nomoto K., 1984, *ApJ*, 277, 791
- O'Donnell J. E., 1994, *ApJ*, 422, 158
- Pastorello A., Zampieri L., Turatto M., Cappellaro E., Meikle W. P. S., Benetti S., Branch D., Baron E., Patat F., Armstrong M., Altavilla G., Salvo M., Riello M., 2004, *MNRAS*, 347, 74
- Patat F., Benetti S., Cappellaro E., Rizzi L., Turatto M., 1999, *IAUC*, 7183, 1
- Pavlovsky C. e. a., 2004, *Advanced Camera for Surveys Instrument Handbook for Cycle 14*. STScI, Baltimore, 5.0 edn
- Pilyugin L. S., Vílchez J. M., Contini T., 2004, *A&A*, 425, 849
- Podsiadlowski P., Joss P. C., 1989, *Nature*, 338, 401
- Podsiadlowski P., Mazzali P. A., Nomoto K., Lazzati D., Cappellaro E., 2004, *ApJL*, 607, L17
- Puckett T., Dowdle G., 2000, *IAUC*, 7507, 2
- Puckett T., Langoussis A., Garrard G. J., 2000, *IAUC*, 7530, 1
- Riess A., Mack J., 2004, Instrument Science Report ACS 2004-006, Time Dependence of ACS WFC CTE Corrections for Photometry and Future Predictions. Space Telescope Science Institute
- Ryder S. D., Sadler E. M., Subrahmanyan R., Weiler K. W., Panagia N., Stockdale C., 2004, *MNRAS*, 349, 1093
- Sarneczky K., Kiss L., Csak B., 1999, *IAUC*, 7154, 3
- Schlegel D. J., Finkbeiner D. P., Davis M., 1998, *ApJ*, 500, 525
- Smartt S. J., Gilmore G. F., Tout C. A., Hodgkin S. T., 2002, *ApJ*, 565, 1089
- Smartt S. J., Gilmore G. F., Trentham N., Tout C. A., Frayn C. M., 2001, *ApJL*, 556, L29
- Smartt S. J., Maund J. R., Gilmore G. F., Tout C. A., Kilkeny D., Benetti S., 2003, *MNRAS*, 343, 735
- Smartt S. J., Maund J. R., Hendry M. A., Tout C. A., Gilmore G. F., Mattila S., Benn C. R., 2004, *Science*, 303, 499
- Stetson P. B., 1987, *PASP*, 99, 191
- Thielemann F.-K., Argast D., Brachwitz F., Hix W. R., Höflich P., Liebendörfer M., Martinez-Pinedo G., Mezzacappa A., Nomoto K., Panov I., 2003, in *From Twilight to Highlight: The Physics of Supernovae Supernova Nucleosynthesis and Galactic Evolution*. pp 331–+
- Turatto M., 2003, *Lecture Notes in Physics*, Berlin Springer Verlag, 598, 21
- Turatto M., Mazzali P. A., Young T. R., et al. 1998, *ApJL*, 498, L129+
- van den Bergh S., Li W., Filippenko A. V., 2003, *PASP*, 115, 1280
- Van Dyk S. D., Li W., Filippenko A. V., 2003, *PASP*, 115, 1
- Van Dyk S. D., Peng C. Y., King J. Y., Filippenko A. V., Treffers R. R., Li W., Richmond M. W., 2000, *PASP*, 112, 1532

- Walborn N. R., Prevot M. L., Prevot L., Wamsteker W.,
Gonzalez R., Gilmozzi R., Fitzpatrick E. L., 1989,
A&A, 219, 229
- Wei J. Y., Cao L., Qiu Y. L., Qiao Q. Y., Hu J. Y., Gu Q. S.,
1999, IAUC, 7124, 1
- Xu D. W., Qiu Y. L., 2001, IAUC, 7555, 2
- Zampieri L., Pastorello A., Turatto M., Cappellaro E.,
Benetti S., Altavilla G., Mazzali P., Hamuy M., 2003,
MNRAS, 338, 711

This figure "sixprog_jrm_v1_fig1.jpg" is available in "jpg" format from:

<http://arxiv.org/ps/astro-ph/0501323v1>

This figure "sixprog_jrm_v1_fig3.jpg" is available in "jpg" format from:

<http://arxiv.org/ps/astro-ph/0501323v1>

This figure "sixprog_jrm_v1_fig4.jpg" is available in "jpg" format from:

<http://arxiv.org/ps/astro-ph/0501323v1>

This figure "sixprog_jrm_v1_fig5.jpg" is available in "jpg" format from:

<http://arxiv.org/ps/astro-ph/0501323v1>

This figure "sixprog_jrm_v1_fig6.jpg" is available in "jpg" format from:

<http://arxiv.org/ps/astro-ph/0501323v1>

This figure "sixprog_jrm_v1_fig7.jpg" is available in "jpg" format from:

<http://arxiv.org/ps/astro-ph/0501323v1>